

# Probing molecular chirality via excitonic nonlinear response\*

Darius Abramavicius<sup>1,2</sup>, Wei Zhuang<sup>3</sup> and Shaul Mukamel<sup>3</sup>

<sup>1</sup> Institute of Physics, Savanoriu Avenue 231, 02300 Vilnius, Lithuania

<sup>2</sup> Theoretical Physics Department, Faculty of Physics of Vilnius University, Sauletekio Avenue 9, Building 3, 10222 Vilnius, Lithuania

<sup>3</sup> Department of Chemistry, University of California Irvine, Irvine, CA 92697-2025, USA

E-mail: [darius.abramavicius@ff.vu.lt](mailto:darius.abramavicius@ff.vu.lt), [wzhuang@uci.edu](mailto:wzhuang@uci.edu) and [smukamel@uci.edu](mailto:smukamel@uci.edu)

Received 15 June 2006, in final form 17 October 2006

Published 23 November 2006

Online at [stacks.iop.org/JPhysB/39/5051](http://stacks.iop.org/JPhysB/39/5051)

## Abstract

The complete set of fifth-rank tensor components which describe the chirality-induced response of excitons to three femtosecond laser pulses is calculated to first order in the optical wavevector, by including the electric dipole and quadrupole and the magnetic dipole contributions to the induced current. The photon echo signal for the  $\pi - \pi^*$  and  $n - \pi^*$  electronic transitions of  $\alpha$  helical polypeptides is calculated using the Green's function solution of the nonlinear exciton equations (NEE). Two-dimensional correlation plots of selected tensor components show considerably enhanced crosspeaks with high sensitivity to structural variations.

(Some figures in this article are in colour only in the electronic version)

## 1. Introduction

The term 'chirality' was coined more than one hundred years ago by Lord Kelvin. According to his definition, any geometrical figure, or group of points is chiral if its image in a plane mirror, ideally realized, cannot be brought to coincide with itself. Chiral systems can therefore be realized in two equally-probable mirror image configurations [1]. Mirror reflection with respect to the  $xy$  plane, can be described by two successive operations: (i) parity  $\mathcal{P}$  (space inversion) and (ii) coordinate system rotation by  $\pi$  around the  $z$  axis. Isotropic ensembles of randomly oriented molecules are invariant to an overall rotation. A racemic mixture of chiral molecules with opposite sense of chirality is invariant to parity whereas an unequal mixture forms an isotropic chiral ensemble. The parity operation transforms between isotropic ensembles with an opposite sense of chirality.

\* This article was originally submitted to the special issue on quantum electrodynamics published in August 2006.

Since the application of two parity operations restores the system back into its original state, all system properties and physical observables, such as optical signal fields  $F$ , can be classified as either parity-even ( $\mathcal{P}F_e = F_e$ ) or parity-odd ( $\mathcal{P}F_o = -F_o$ ) [2, 3]. Parity-odd signals change sign for chiral ensembles with opposite chirality and, therefore, vanish for non-chiral systems and racemates (equal mixtures of chiral molecules with opposite chirality). Parity-even signals, in contrast, are not sensitive to the sense of chirality. We shall denote the two types of signals as chirality-induced (CI) and non-chiral (NC), respectively.

Circularly polarized light is chiral since it has either left (L) or right (R) screw symmetry with respect to the propagation direction. The simplest chirality-induced linear optical technique, circular dichroism (CD), measures the difference between absorption of L and R circularly polarized light [4, 5]. Thanks to its high structural sensitivity, the technique has been extensively applied to protein secondary structure determination using electronic transitions in the UV [6–9] and vibrational transitions in the IR [10–12]. Raman optical activity (ROA) is a closely related technique which measures the difference between resonant scattering of L and R light [2, 13, 14].

Nonlinear CI techniques have been developed as well. The chirality of interfaces of liquids and solids where the surface layer of molecules has some degree of order, has been studied using second-order techniques [15] such as sum-frequency generation (SFG) and second harmonic generation (SHG) [16–18]. CI tensor elements of the second-order susceptibility  $\chi^{(2)}$  have been determined for specific molecular geometries [19–21]. Second-order techniques can also be used to study chirality in bulk samples; however, these signals are very weak due to phase mismatching [22, 23]. Macroscopic transmission/reflection tensors of the bulk have been used to describe the chirality [24].

In this paper we use microscopic response tensors to study chirality effects in ultrafast third-order techniques, which can monitor dynamical events, including protein folding and denaturation, molecular twisting, chemical bond breaking and excited state relaxation pathways. Coherent techniques such as the photon-echo can discriminate between homogeneous and inhomogeneous contributions to highly congested lineshapes by tracking correlated fluctuations of Hamiltonian parameters [25–29]. Pump–probe and transient grating spectra can follow exciton populations, as well as charge transport, separation and recombination [30, 31]. Vibrational nonlinear optical techniques were recently applied to study protein structure and folding dynamics [32] and hydrogen bonding fluctuations in water [33, 34]. Resonance Raman spectra probe vibrational transitions coupled to specific electronic resonances [35–37]. Two-dimensional third-order optical techniques reveal fine details unavailable from linear spectroscopy [27, 29, 32, 38–41]: overlapping transitions in the absorption spectrum can be separated by dispersing them in two dimensions, and additional information about the dynamics may be extracted from the lineshapes. The ellipticity of peak patterns in 2D plots, and the elongation directions of these ellipses reflect bath correlations at different parts of the system and their timescales [42–44].

The odd-order (linear, third-order, etc) CI response functions are first order in the optical wavevector and may be distinguished by the specific configurations of optical field polarizations [45]. Our previous studies were limited to the three independent CI tensor components of the third-order response in a collinear field configuration [46, 47]. Here we present the complete set of tensor components for collinear and non-collinear configurations.

The electrodynamics of a molecule coupled to the optical field is usually described by either the  $p \cdot A$  (minimal coupling) Hamiltonian which couples the momentum with the vector potential of the field, or the  $\mu \cdot E$  or multipolar Hamiltonian which describes the interaction between the system multipoles and the optical electric and magnetic fields. The two Hamiltonians are related by the Power–Zienau canonical transformation [48–51]. The

multipolar Hamiltonian for time-dependent fields can be alternatively obtained by expanding the  $p \cdot A$  Hamiltonian field variables in the coordinate [52]. We will adopt the  $p \cdot A$  Hamiltonian in this paper since it allows a more compact description of the combined electric and magnetic response [46, 53].

Our results are illustrated by simulations of the photon echo signal of a polypeptide in the 180–250 nm region originating mostly from the  $\pi - \pi^*$  NV1 and NV2 and the  $n - \pi^*$  [7, 9, 54, 55] electronic transitions along the protein backbone. NV1 and NV2 possess a large transition dipole moment and dominate the linear absorption. The  $n - \pi^*$  transition has a magnetic but no electric transition dipole and is thus only seen in optical activity measurements. The CD spectra of proteins in this region consist of several overlapping transitions. They are very sensitive to backbone geometry and can distinguish between  $\alpha$  helix,  $\beta$  sheet and polyProII helix secondary structure motifs [7, 56]. As found earlier for CI vibrational nonlinear techniques, the crosspeaks which originate from couplings between different units are amplified in third-order CI signals [47]. We explore the sensitivity of the third-order CI signals to variations in molecular structure.

## 2. The exciton model and Green's functions

We consider an assembly of interacting localized electronic chromophores where the  $m$ 'th chromophore has several electronic excited states  $a, b \dots$  with excitation frequencies  $\varepsilon_{ma}$ . We assume that the only allowed optical transitions are between the ground state  $g$  and the excited states and that no direct transitions between the excited states of the same chromophore are allowed. The system is described by the Frenkel exciton Hamiltonian

$$\hat{H} = \sum_{mn,ab} h_{ma,nb} \hat{B}_{ma}^\dagger \hat{B}_{nb} + \hat{H}', \quad (1)$$

where  $h_{ma,ma} \equiv \varepsilon_{ma}$ , and  $h_{ma,ng} \equiv 0$ ; the ground state energy is 0. The Frenkel exciton model is extensively used for describing optical properties of coupled chromophores in e.g. molecular crystals, polymers, molecular aggregates and proteins [57, 58].  $\hat{B}_{ma}^\dagger$  and  $\hat{B}_{ma}$  are the exciton creation and annihilation operators for an excitation of mode  $a$  of chromophore  $m$ . The commutation relations  $[\hat{B}_{ma}, \hat{B}_{nb}^\dagger] = \delta_{mn} \delta_{ab} (1 - \sum_{c=1}^M \hat{B}_{mc}^\dagger \hat{B}_{mc}) - \delta_{mn} \hat{B}_{nb}^\dagger \hat{B}_{ma}$  where  $M$  is the number of excited states of each chromophore [59] ensure Pauli exclusion.  $h_{ma,nb}$  is the intermode excitonic coupling in the Heitler–London approximation i.e. off resonant  $\hat{B}^\dagger \hat{B}^\dagger$  and  $\hat{B} \hat{B}$  terms are neglected; the ground state of the system is the vacuum state. Vibrational excitons can be described by a similar Hamiltonian with Boson operators [59].

We next review the relevant exciton states. The linear response depends solely on the single-exciton eigenstates  $\psi_{\xi,ma}$  and their energies  $E_\xi$ , obtained by diagonalizing the one-exciton block of the Hamiltonian:

$$\sum_{nb} h_{ma,nb} \psi_{\xi,nb} = E_\xi \psi_{\xi,ma}. \quad (2)$$

The excited state evolution is described by Green's functions. We define the retarded one-exciton Green's function,  $G(t)$ ,  $\langle \hat{B}_{ma} \rangle_t = G_{ma,nb}(t) \langle \hat{B}_{nb} \rangle_0$ . Switching to the frequency-domain  $[F(\mathbf{r}, t) = \frac{1}{(2\pi)^4} \int d\mathbf{k} \int d\omega F(\mathbf{k}, \omega) e^{i\mathbf{k}\mathbf{r} - i\omega t}]$  we have

$$G_{ma,nb}(\omega) = \sum_{\xi} \psi_{\xi,ma} I_{\xi}(\omega) \psi_{\xi,nb}^*, \quad (3)$$

with

$$I_{\xi}(\omega) = \frac{i}{\omega - E_{\xi} + i\gamma_{\xi}}, \quad (4)$$

where  $\gamma_\xi$  is the dephasing rate of the  $\xi$  exciton. Third-order techniques probe the two-exciton states as well. The two-exciton Green's function,  $\mathcal{G}^{(2)}(t)$ , is defined by  $\langle \hat{B}_{ma} \hat{B}_{nb} \rangle_t = \mathcal{G}_{manb,m'a'n'b'}^{(2)}(t) \langle \hat{B}_{m'a'} \hat{B}_{n'b'} \rangle_0$ .

The nonlinear exciton equations (NEE) [59–61] allow us to calculate the signals while avoiding the expensive explicit calculation of the two-exciton Green's functions; their effect is introduced through a one-exciton quasiparticle scattering. These equations are particularly suitable for large scale simulations [45, 60]. Using the NEE framework, the two-exciton Green's function is obtained using the Bethe Salpeter equation in the frequency domain:

$$\mathcal{G}^{(2)}(\omega) = \mathcal{G}(\omega) + \mathcal{G}(\omega)\Gamma(\omega)\mathcal{G}(\omega), \quad (5)$$

where  $\mathcal{G}_{manb,m'a'n'b'}(\omega) = i \sum_{\xi\xi'} \psi_{\xi,ma} \psi_{\xi',nb} [\omega - E_\xi - E_{\xi'} + i(\gamma_\xi + \gamma_{\xi'})]^{-1} \psi_{\xi,m'a'}^* \psi_{\xi',n'b'}^*$  is the noninteracting two-exciton Green's function and  $\Gamma(\omega)$  is the two-exciton scattering matrix.  $U(z)$  and  $\mathbf{1}$  are square matrices of size  $MN \times MN$ , where  $N$  is the number of chromophores and  $M$  is the number of excited states of each chromophore.  $\mathbf{1}_{ma,nb} = \delta_{mn} \delta_{ab}$  is the unit matrix.  $U_{ma,nb} = z \delta_{mn}$  shifts the double-exciton energy by  $z$  from  $\varepsilon_{ma} + \varepsilon_{nb}$  (soft-core boson model). To represent coupled two-level chromophores we set  $z \rightarrow \infty$ . The soft-core then becomes a hard-core boson model, where two excitations cannot reside on the same chromophore (Pauli exclusion). The two-exciton scattering matrix for hard-core bosons is

$$\Gamma(\omega) = -i \lim_{z \rightarrow \infty} U(z)(\mathbf{1} + i\mathcal{G}(\omega)U(z))^{-1}. \quad (6)$$

Numerically the limit  $z \rightarrow \infty$  is realized by taking  $z \gg 2E_\xi$ .

### 3. The chirality-induced signals

Using the minimal-coupling Hamiltonian, the interaction of a system of point charges with the electromagnetic field is given by

$$\hat{H}^I(t) = \sum_{\alpha} \frac{-q_{\alpha}}{cm_{\alpha}} \hat{\mathbf{p}}_{\alpha}(t) \cdot \hat{\mathbb{A}}(\mathbf{r}_{\alpha}, t) + \frac{q_{\alpha}^2}{2m_{\alpha}c^2} \hat{\mathbb{A}}^2(\mathbf{r}_{\alpha}, t), \quad (7)$$

where  $\sum_{\alpha}$  runs over all charged particles (electrons when describing electronic excitations and nuclei for vibrational excitations),  $q_{\alpha}$  is the charge of particle  $\alpha$ , with mass  $m_{\alpha}$ , and  $\hat{\mathbb{A}}$  is the electromagnetic vector potential operator. This interaction Hamiltonian can be recast using the electric current  $\hat{\mathbb{J}}(\mathbf{r}, t)$  and charge density  $\hat{Q}(\mathbf{r}, t)$  operators [49, 51, 53]. In the semiclassical approximation where the vector potential operator is replaced by its expectation value we have

$$\hat{H}^I(t) = -\frac{1}{c} \int d\mathbf{r} [\hat{\mathbb{J}}(\mathbf{r}, t) \cdot \mathbb{A}(\mathbf{r}, t) + \hat{Q}(\mathbf{r}, t) \mathbb{A}^2(\mathbf{r}, t)]. \quad (8)$$

We shall use the Coulomb gauge where the vector potential  $\mathbb{A}(\mathbf{r}, t)$  is transverse.

The Frenkel exciton model is defined in terms of localized (non-overlapping) many-electron eigenfunctions of isolated chromophores. We introduce the wavefunction of molecular state  $a$  of chromophore  $m$  as  $\phi_{ma}$ . The wavefunction of the excitonic ground state is then  $|0\rangle \equiv \Pi_m \phi_{mg}$  where  $g$  indicates the ground state, while the wavefunction of the excited state  $\hat{B}_{ma}^{\dagger}|0\rangle \equiv \phi_{ma} \Pi_{n \neq m} \phi_{ng}$ . The excitonic current–density operator will be given by

$$\hat{\mathbb{J}}(\mathbf{r}) = \sum_{ma} (\bar{\mathbf{j}}_{ma}^*(\mathbf{r}) \hat{B}_{ma}^{\dagger} + \bar{\mathbf{j}}_{ma}(\mathbf{r}) \hat{B}_{ma}), \quad (9)$$

where  $\bar{\mathbf{j}}_{ma}(\mathbf{r})$  is the transition current density ( $c$  number) of transition  $g \rightarrow a$  of chromophore  $m$ . Transition current densities of different chromophores do not overlap and are localized in

the vicinity of the chromophores. The sum runs over all chromophores and transitions, all assumed to originate from the ground state, thus the index  $g$  is omitted. When transitions between the excited states are included the induced current operator would include terms like  $\hat{B}_{ma}^{\dagger 2}$ ,  $\hat{B}_{ma}^{\dagger} \hat{B}_{mb}$  and their conjugates. They are neglected here. The transition currents will be calculated using an electric and magnetic multipolar expansion of the chromophores.

In  $\mathbf{k}$  space the interaction Hamiltonian is

$$\hat{H}'(t) = -\frac{1}{c} \int \frac{d\mathbf{k}}{(2\pi)^3} \left[ \hat{\mathbb{J}}(-\mathbf{k}, t) \cdot \hat{\mathbb{A}}(\mathbf{k}, t) + \int \frac{d\mathbf{k}'}{(2\pi)^3} \hat{Q}(-\mathbf{k} - \mathbf{k}', t) \hat{\mathbb{A}}(\mathbf{k}, t) \hat{\mathbb{A}}(\mathbf{k}', t) \right]. \quad (10)$$

In the Heisenberg representation we have the following relation between the current density  $\hat{\mathbb{J}}$ , total electric polarization  $\hat{\mathbb{P}}$ , and magnetization  $\hat{\mathbb{M}}$  [50]:

$$\hat{\mathbb{J}}(\mathbf{k}\omega) = -i\omega \hat{\mathbb{P}}(\mathbf{k}\omega) - i\mathbf{k} \times \hat{\mathbb{M}}(\mathbf{k}\omega). \quad (11)$$

The total polarization operator is responsible for charge displacements, whereas the magnetization is related to the angular momentum. When chromophore size is much smaller than optical wavelength, to first order in the optical wavevector  $\mathbf{k}$  we only need to retain the electric dipole,  $\boldsymbol{\mu}$ , the electric quadrupole,  $\mathbf{Q}$ , and the magnetic dipole  $\mathbf{m}$  of each chromophore. We introduce these parameters in the excitonic basis set.  $\bar{\boldsymbol{\mu}}_{ma}(\mathbf{r}) \equiv \boldsymbol{\mu}_{ma} \delta(\mathbf{r} - \mathbf{r}_m)$  is the transition dipole density of chromophore  $m$ , where  $\boldsymbol{\mu}_{ma} = \langle \phi_{ma} | \sum_{\alpha} q_{\alpha} (\mathbf{r}_{\alpha} - \mathbf{r}_m) | \phi_{mg} \rangle$  is the transition dipole localized at the chromophore position  $\mathbf{r}_m$ .  $\bar{\mathbf{Q}}_{ma}(\mathbf{r}) \equiv \mathbf{Q}_{ma} \delta(\mathbf{r} - \mathbf{r}_m)$  is the transition quadrupole density.  $\mathbf{Q}_{ma} = \langle \phi_{ma} | \sum_{\alpha} \frac{q_{\alpha}}{2} (\mathbf{r}_{\alpha} - \mathbf{r}_m) \otimes (\mathbf{r}_{\alpha} - \mathbf{r}_m) | \phi_{mg} \rangle$  is the corresponding transition quadrupole.  $\bar{\mathbf{m}}_{ma}(\mathbf{r}) \equiv \mathbf{m}_{ma} \delta(\mathbf{r} - \mathbf{r}_m)$  is the magnetic transition density, where  $\mathbf{m}_{ma} = \langle \phi_{ma} | \sum_{\alpha} \frac{q_{\alpha}}{2mc} (\mathbf{r}_{\alpha} - \mathbf{r}_m) \times \mathbf{p}_{\alpha} | \phi_{mg} \rangle$  is the magnetic transition dipole.  $\mathbf{r}_{\alpha}$  is the coordinate operator, and  $\mathbf{p}_{\alpha} = -i\hbar \nabla_{\alpha}$  is the momentum of electron  $\alpha$ .  $\boldsymbol{\mu}_{ma}$ ,  $\mathbf{Q}_{ma}$  and  $\mathbf{m}_{ma}$  are associated with isolated chromophores in a chromophore-based coordinate frames. Using equation (11) the transition current can be related to the electric and magnetic transition dipoles, and quadrupoles:

$$\bar{\mathbf{j}}_{ma}(-\mathbf{k}) = -i\omega \bar{\boldsymbol{\mu}}_{ma}(-\mathbf{k}) - \omega \bar{\mathbf{Q}}_{ma}(-\mathbf{k}) \cdot \mathbf{k} - i\mathbf{k} \times \bar{\mathbf{m}}_{ma}(-\mathbf{k}), \quad (12)$$

where  $\bar{\mathbf{j}}_{ma}(\mathbf{k}) = \int d\mathbf{r} \bar{\mathbf{j}}_{ma}(\mathbf{r}) \exp(-i\mathbf{k} \cdot \mathbf{r})$ ,  $\bar{\boldsymbol{\mu}}_{ma}(\mathbf{k}) = \boldsymbol{\mu}_{ma} \exp(i\mathbf{k} \cdot \mathbf{r}_m)$ ,  $\bar{\mathbf{Q}}_{ma}(\mathbf{k}) = \mathbf{Q}_{ma} \exp(i\mathbf{k} \cdot \mathbf{r}_m)$  and  $\bar{\mathbf{m}}_{ma}(\mathbf{k}) = \mathbf{m}_{ma} \exp(i\mathbf{k} \cdot \mathbf{r}_m)$ .

Expanding  $\bar{\mathbf{j}}_{ma}(\mathbf{k})$  to first order in  $\mathbf{k}$  we get

$$\bar{\mathbf{j}}_{ma}(-\mathbf{k}) \approx -i\omega \boldsymbol{\mu}_{ma} - \omega (\mathbf{k} \cdot \mathbf{r}_m) \boldsymbol{\mu}_{ma} - \omega \mathbf{Q}_{ma} \cdot \mathbf{k} + i\mathbf{k} \times \mathbf{m}_{ma}. \quad (13)$$

The first term represents the dipole approximation for the entire system, the second gives rise to inter-chromophore quadrupole moments whereas the third and the fourth terms represent intra-chromophore quadrupole and magnetic moments. The first term is zeroth order in the wavevector whereas the other terms are first order. For aggregates made out of non-chiral chromophores, only the excitonic chirality (the second term) contributes to first order in  $\mathbf{k}$ . This contribution increases as the excitons become more delocalized. The other contributions increase linearly with size, but due to excitonic cooperativity we expect the second term to increase more rapidly. Therefore even when the chromophores are chiral, the second term may be dominant for large excitonic couplings.

In a four-wave-mixing experiment (figure 1), three laser fields interact with the sample. The induced polarization and magnetization then result in a molecular current,  $\mathbb{J}$ , which serves

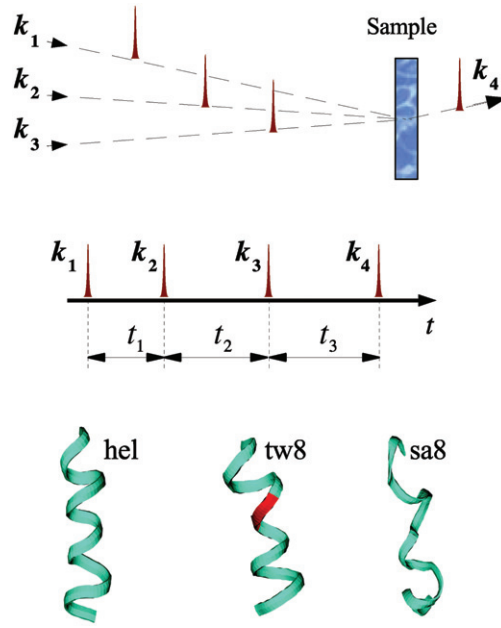


**Figure 1.** Top and middle: a three-pulse time-domain four-wave-mixing experiment. The time ordered pulses have wavevectors  $\mathbf{k}_1$ ,  $\mathbf{k}_2$ ,  $\mathbf{k}_3$ .  $\mathbf{k}_1$  comes first followed by  $\mathbf{k}_2$  and then  $\mathbf{k}_3$ ; the signal is generated along  $\mathbf{k}_4$ .  $t_j$  are the time delays. Bottom: the three helices used in the simulations. hel is an unperturbed 17 residue helix, tw8 is twisted helix in the red region, sa8 is twisted helix after simulated annealing.

as a source in Maxwell's equations for the signal electric field  $\mathbb{E}$ :

$$\nabla \times \nabla \times \mathbb{E} + \frac{1}{c^2} \frac{\partial^2}{\partial t^2} \mathbb{E} = -\frac{4\pi}{c^2} \frac{\partial \mathbb{J}}{\partial t}. \quad (14)$$

We shall consider impulsive time-domain experiments performed with three temporally well-separated pulses where time ordering of the various interactions is strictly enforced. These signals are generated by a single interaction with each pulse. Only the linear couplings in the vector potential (equation (8)) contribute in this case. The quadratic  $\mathbb{A}^2$  term gives an additional contributions to the complete response function [53].

Linear optical signals are described by the linear susceptibility, which for our model is given by [46]

$$\chi_{\nu_S \nu_1}^{(1)}(-\mathbf{k}_S, -\omega_S; \mathbf{k}_1, \omega_1) = 2\pi \frac{i}{\omega_1^2} \delta(\omega_S - \omega_1) \sum_{\xi} \langle \bar{j}_{\xi}^{\nu_S}(-\mathbf{k}_S) \bar{j}_{\xi}^{*\nu_1}(-\mathbf{k}_1) \rangle I_{\xi}(\omega_1) + \text{c.c.}' \quad (15)$$

Here  $\bar{j}_{\xi}(\mathbf{k}) \equiv \sum_{ma} \psi_{\xi(ma)} \bar{j}_{ma}(\mathbf{k})$  and c.c.' implies changing the signs of all frequencies and wavevectors and then taking complex conjugate. This susceptibility is given in terms of the one-exciton states  $\xi$ , obtained by diagonalizing the one-exciton block of the system Hamiltonian (equation (2)).  $\chi^{(1)}$  relates the induced current with wavevector  $\mathbf{k}_S$ , frequency  $\omega_S$  and polarization  $\nu_S$ , to the incoming field with  $\mathbf{k}_1$ ,  $\omega_1$  and  $\nu_1$ . All linear signals are described by this susceptibility: the linear absorption is  $\sigma_A \propto \omega \text{Im}(\chi_{xx}^{(1)}(-\mathbf{k}, -\omega, \mathbf{k}, \omega))$ , and the circular dichroism is  $\sigma_{CD} \propto \omega \text{Im}(i\chi_{xy}^{(1)}(-\mathbf{k}, -\omega, \mathbf{k}, \omega))$ .

The orientationally-averaged  $\langle \bar{\mathbf{j}}_{\xi}^{\nu_S}(-\mathbf{k}_S) \bar{\mathbf{j}}_{\xi}^{\nu_1}(-\mathbf{k}_1) \rangle$  factors to first order in the wavevector depend on the field polarizations as well as their wavevectors:

$$\langle \bar{\mathbf{j}}_{\xi}^{\nu_S}(-\mathbf{k}_S) \bar{\mathbf{j}}_{\xi}^{\nu_1}(-\mathbf{k}_1) \rangle = \omega^2 \frac{1}{3} [(\boldsymbol{\nu}_S \cdot \boldsymbol{\nu}_1) |\boldsymbol{\mu}_{\xi}|^2 - \mathbf{i} \mathbf{k}_1 \cdot (\boldsymbol{\nu}_S \times \boldsymbol{\nu}_1) (\boldsymbol{\mu}_{\xi} \odot \mathbf{q}_{\xi} - 2\mathbf{m}_{\xi}'' \cdot \boldsymbol{\mu}_{\xi})], \quad (16)$$

where

$$\begin{aligned} \mathbf{m}_{\xi}'' &= \frac{\lambda}{2\pi} \sum_{ma} \psi_{\xi(ma)} \text{Im } \mathbf{m}_{ma}, \\ \boldsymbol{\mu}_{\xi} &= \sum_{ma} \psi_{\xi(ma)} \boldsymbol{\mu}_{ma}, \\ \mathbf{q}_{\xi}^{\nu_2\nu_1} &= \sum_{ma} \psi_{\xi(ma)} (\mathbf{r}_m^{\nu_2} \boldsymbol{\mu}_{ma}^{\nu_1} + \mathbf{Q}_{ma}^{\nu_2\nu_1}); \end{aligned}$$

$\boldsymbol{\nu}$  is the lab frame unit vector, and we define  $\boldsymbol{\mu} \odot \mathbf{q} \equiv \sum_{\alpha_3\alpha_2\alpha_1=x,y,z} \epsilon_{\alpha_3\alpha_2\alpha_1} \boldsymbol{\mu}^{\alpha_3} \mathbf{q}^{\alpha_2\alpha_1}$  ( $\epsilon_{\alpha_3\alpha_2\alpha_1}$  is the antisymmetric Levi-Civita tensor). Here  $\mathbf{k}_S = \mathbf{k}_1$ , and orientational averaging is performed using the expressions of appendix A. We also note that the CD spectrum does not depend on the quadrupole moment if  $\mathbf{q}^{\nu_1\nu_2} = \mathbf{q}^{\nu_2\nu_1}$  since in this case it vanishes upon orientational averaging due to the Levi-Civita tensor  $\epsilon_{\nu_3\nu_2\nu_1}$ .

We consider an impulsive coherent resonant time-domain experiment carried out with short non-overlapping pulses [46, 47]. This three-dimensional signal, which depends on the three delay times  $t_3, t_2, t_1$ , will be displayed by performing a one-sided Fourier transform [ $f(\Omega) = \int_0^{\infty} dt e^{i\Omega t} f(t)$ ] with respect to the delay times  $t_1$  and  $t_3$  with the conjugate frequencies  $\Omega_1$  and  $\Omega_3$ , and  $t_2$  is held fixed. The response function,  $\mathbb{R}_{\nu_S\nu_3\nu_2\nu_1}^{(3)}(\mathbf{k}_S, \Omega_3, t_2, \Omega_1)$  relates the induced current with wavevector  $\mathbf{k}_S$  and polarization  $\nu_S$  to the incoming pulses with wavevectors  $\mathbf{k}_j$  and polarizations  $\nu_j$ . Both real and imaginary parts of  $\mathbb{R}$  can be measured separately by heterodyne detection [50]. Phase-matching gives several independent signals with wavevectors  $\mathbf{k}_S = u\mathbf{k}_1 + v\mathbf{k}_2 + w\mathbf{k}_3$ ; here  $u, v$  and  $w$  are integers. We focus on the  $\mathbf{k}_I = -\mathbf{k}_1 + \mathbf{k}_2 + \mathbf{k}_3$  (photon echo) technique and set  $t_2 = +0$ . The corresponding response function is [46]

$$\begin{aligned} \mathbb{R}_{\nu_4\nu_3\nu_2\nu_1}^{\mathbf{k}_I}(\Omega_3, t_2 = 0, \Omega_1) &= -2 \frac{i^3}{c^3 \omega^4} \sum_{\xi_4 \dots \xi_1} \langle \bar{\mathbf{j}}_{\xi_4}^{\nu_4}(-\mathbf{k}_I) \bar{\mathbf{j}}_{\xi_3}^{\nu_3}(-\mathbf{k}_3) \bar{\mathbf{j}}_{\xi_2}^{\nu_2}(-\mathbf{k}_2) \bar{\mathbf{j}}_{\xi_1}^{\nu_1}(-\mathbf{k}_1) \rangle \\ &\times I_{\xi_1}^*(-\Omega_1) I_{\xi_4}(\Omega_3) \Gamma_{\xi_4\xi_1\xi_3\xi_2}(\Omega_3 + E_{\xi_1} + i\gamma_{\xi_1}) \mathcal{I}_{\xi_3\xi_2}(\Omega_3 + E_{\xi_1} + i\gamma_{\xi_1}), \end{aligned} \quad (17)$$

where  $\Gamma_{\xi_4\xi_3\xi_2\xi_1} = \sum_{n_4n_3n_2n_1} \psi_{\xi_4n_4}^* \psi_{\xi_3n_3}^* \Gamma_{n_4n_3n_2n_1} \psi_{\xi_2n_2} \psi_{\xi_1n_1}$  is the scattering matrix in the one-exciton basis.

Assuming  $\omega_2 \approx \omega_1 \approx \omega$  where  $\omega$  is the mean optical frequency, the orientational factor for the third-order response becomes

$$\begin{aligned} \langle \bar{\mathbf{j}}_{\xi_4}^{\nu_4}(-\mathbf{k}_4) \bar{\mathbf{j}}_{\xi_3}^{\nu_3}(s_3, -\mathbf{k}_3) \bar{\mathbf{j}}_{\xi_2}^{\nu_2}(s_2, -\mathbf{k}_2) \bar{\mathbf{j}}_{\xi_1}^{\nu_1}(s_1, -\mathbf{k}_1) \rangle &= -s_3 s_2 s_1 \omega^4 \left\{ \langle \boldsymbol{\mu}_{\xi_4}^{\nu_4} \boldsymbol{\mu}_{\xi_3}^{\nu_3} \boldsymbol{\mu}_{\xi_2}^{\nu_2} \boldsymbol{\mu}_{\xi_1}^{\nu_1} \rangle \right. \\ &+ i \sum_{\nu_5} \left[ -\mathbf{k}_4^{\nu_5} \langle \boldsymbol{q}_{\xi_4}^{\nu_5, \nu_4} \boldsymbol{\mu}_{\xi_3}^{\nu_3} \boldsymbol{\mu}_{\xi_2}^{\nu_2} \boldsymbol{\mu}_{\xi_1}^{\nu_1} \rangle + s_3 \mathbf{k}_3^{\nu_5} \langle \boldsymbol{\mu}_{\xi_4}^{\nu_4} \boldsymbol{q}_{\xi_3}^{\nu_5, \nu_3} \boldsymbol{\mu}_{\xi_2}^{\nu_2} \boldsymbol{\mu}_{\xi_1}^{\nu_1} \rangle \right. \\ &+ s_2 \mathbf{k}_2^{\nu_5} \langle \boldsymbol{\mu}_{\xi_4}^{\nu_4} \boldsymbol{\mu}_{\xi_3}^{\nu_3} \boldsymbol{q}_{\xi_2}^{\nu_5, \nu_2} \boldsymbol{\mu}_{\xi_1}^{\nu_1} \rangle + s_1 \mathbf{k}_1^{\nu_5} \langle \boldsymbol{\mu}_{\xi_4}^{\nu_4} \boldsymbol{\mu}_{\xi_3}^{\nu_3} \boldsymbol{\mu}_{\xi_2}^{\nu_2} \boldsymbol{q}_{\xi_1}^{\nu_5, \nu_1} \rangle \left. \right] \\ &+ i \sum_{\nu_5\alpha} \left[ -\epsilon_{\nu_4\nu_3\alpha} \mathbf{k}_4^{\nu_5} \langle \mathbf{m}_{\xi_4}^{\prime\prime\alpha} \boldsymbol{\mu}_{\xi_3}^{\nu_3} \boldsymbol{\mu}_{\xi_2}^{\nu_2} \boldsymbol{\mu}_{\xi_1}^{\nu_1} \rangle + s_3 \epsilon_{\nu_3\nu_2\alpha} \mathbf{k}_3^{\nu_5} \langle \boldsymbol{\mu}_{\xi_4}^{\nu_4} \mathbf{m}_{\xi_3}^{\prime\prime\alpha} \boldsymbol{\mu}_{\xi_2}^{\nu_2} \boldsymbol{\mu}_{\xi_1}^{\nu_1} \rangle \right. \\ &\left. + s_2 \epsilon_{\nu_2\nu_1\alpha} \mathbf{k}_2^{\nu_5} \langle \boldsymbol{\mu}_{\xi_4}^{\nu_4} \boldsymbol{\mu}_{\xi_3}^{\nu_3} \mathbf{m}_{\xi_2}^{\prime\prime\alpha} \boldsymbol{\mu}_{\xi_1}^{\nu_1} \rangle + s_1 \epsilon_{\nu_1\nu_0\alpha} \mathbf{k}_1^{\nu_5} \langle \boldsymbol{\mu}_{\xi_4}^{\nu_4} \boldsymbol{\mu}_{\xi_3}^{\nu_3} \boldsymbol{\mu}_{\xi_2}^{\nu_2} \mathbf{m}_{\xi_1}^{\prime\prime\alpha} \rangle \right] \left. \right\}, \end{aligned} \quad (18)$$

where  $s_j = \pm 1$  and we used the notation  $\bar{\mathbf{j}}_{\xi}^{\nu}(+1, \mathbf{k}) \equiv \bar{\mathbf{j}}_{\xi}^{\nu}(\mathbf{k})$  and  $\bar{\mathbf{j}}_{\xi}^{\nu}(-1, \mathbf{k}) \equiv \bar{\mathbf{j}}_{\xi}^{\nu}(\mathbf{k})$ . Equation (18) can be calculated by orientational averaging of tensor products of arbitrary

sets of fixed vectors and second-rank tensors defined in the molecular frame, as shown in the appendix.

The orientational factors given by equations (A.5)–(A.18) relate the signals to molecular geometry. The CI terms can be identified by examining the products of transition dipoles. The electric transition dipole  $\mu_\xi$  and coordinate  $\mathbf{r}_m$  are parity-odd, while the magnetic transition dipole,  $\mathbf{m}_\xi$  and tensors  $\mathbf{q}_\xi$  are even. By performing the parity operation on the susceptibilities and inspecting the parity symmetry we can connect the susceptibility with the chirality. All zero order in wavevector contributions to odd (linear and cubic) response are NC since they involve either two or four electric transition dipoles. The corresponding first-order contributions in wavevectors are CI. The signals will depend on the specific laser pulse geometry. By decomposing all wavevectors and polarization vectors into elementary components we get the tensor contributions to the signal. We next consider these contributions.

As shown by Andrews and Thirunamachandran [62], the column-vectors  $F_{\{v\}}^{(n)}$  (see equations (A.10) and (A.11)) give the linearly-independent contributions to the averaged response tensors. By inspecting the orientationally-averaged expressions we get the independent nonvanishing elements of the orientational tensors. We define the lab frame by assuming that the signal propagates along  $z$  and is  $x$  polarized. We also note that all fields  $j = 1, 2, 3, s$  are transverse so that  $\mathbb{E}_j \cdot \mathbf{k}_j = 0$ . The polarization unit vector is  $\mathbf{e}_j$  and the unit wavevector is  $\boldsymbol{\kappa}_j$ . We will use polarizations and wavevectors which coincide with the lab frame unit vectors  $\mathbf{e}_j = \boldsymbol{\nu}_j \equiv \mathbf{x}, \mathbf{y}, \mathbf{z}$ . We shall denote the polarization and wavevector configurations of the various possible techniques by  $\nu_4\nu_3\nu_2\nu_1(\alpha_4\alpha_3\alpha_2\alpha_1)$ ; here  $\nu_j = x, y, z$  is the polarization direction of field  $j$  and  $\alpha_j$  is its wavevector direction. The fields are ordered chronologically from right to left (field 1 comes first, field 4 (signal) is the last).

We first consider the wavevector-independent (dipole approximation) contribution. The column-vector  $F_{\{v\}}^{(4)}$  identifies three independent components:  $F_{\{v\}}^{(4)} = (1, 0, 0)^T$ ,  $F_{\{v\}}^{(4)} = (0, 1, 0)^T$  and  $F_{\{v\}}^{(4)} = (0, 0, 1)^T$ . We next need to find field configurations that give only one contribution out of the three.  $F_{\{v\}}^{(4)} = (1, 0, 0)^T$  requires  $\mathbf{e}_4 = \mathbf{e}_3$  and  $\mathbf{e}_2 = \mathbf{e}_1$  and  $(\mathbf{e}_4 \cdot \mathbf{e}_2)(\mathbf{e}_3 \cdot \mathbf{e}_1) = (\mathbf{e}_4 \cdot \mathbf{e}_1)(\mathbf{e}_3 \cdot \mathbf{e}_2) = 0$ . This can be realized for instance when  $\mathbf{e}_4 = \mathbf{e}_3 = \mathbf{x}$  and  $\mathbf{e}_2 = \mathbf{e}_1 = \mathbf{y}$ . We choose  $\nu_4\nu_3\nu_2\nu_1 \equiv xxyy$  to represent  $F_{\{v\}}^{(4)} = (1, 0, 0)^T$  (this choice is not unique). The other two independent contributions are obtained in the configurations  $xyxy$  giving  $F_{\{v\}}^{(4)} = (0, 1, 0)^T$  and  $xyyx$  giving  $F_{\{v\}}^{(4)} = (0, 0, 1)^T$ . All other possible configurations are obtained as linear combinations of  $xxyy$ ,  $xyxy$  and  $xyyx$ . For instance,  $xxxx$  gives  $F_{\{v\}}^{(4)} = (1, 1, 1)^T \equiv (1, 0, 0)^T + (0, 1, 0)^T + (0, 0, 1)^T$  and therefore  $\mathbb{R}_{xxxx} = \mathbb{R}_{xyxy} + \mathbb{R}_{xyxy} + \mathbb{R}_{xyyx}$ .

We next turn to  $F_{\{v\}}^{(5)}$  (equation (A.11)). This six-row column-vector implies that there are six linearly independent contributions. We need to find field configurations that select one contribution out of the six. Using our signal configuration ( $\mathbf{e}_4 = \mathbf{x}$  and  $\boldsymbol{\kappa}_4 = \mathbf{z}$ ) a vector  $F_{\{v\}}^{(5)} = (1, *, *, *, *, 0)^T$  (here ‘\*’ is either 0 or 1) is obtained by setting  $\mathbf{e}_3 = \mathbf{y}$  and  $\mathbf{e}_2 = \mathbf{z}$  and  $\mathbf{e}_1 = \boldsymbol{\kappa}_j$ . The choice of  $\mathbf{e}_1 = \mathbf{x}$ ,  $\boldsymbol{\kappa}_j = \pm\mathbf{x}$ , leads to the polarization tensor  $xyzx$ , and results in  $F_{\{v\}}^{(5)} = (\pm 1, 0, 0, 0, 0, 0)^T$ , which is one of the six linearly independent contributions. Since these contributions involve wavevectors, the next step is to determine possible wavevector directions which enter  $F_{\{v\}}^{(5)} = (\pm 1, 0, 0, 0, 0, 0)^T$ . Since  $\boldsymbol{\kappa}_j = \pm\mathbf{x}$ , only wavevectors parallel to  $x$  direction contribute. There is only one wavevector configuration consistent with the phase matching direction ( $\mathbf{k}_4 = \mathbf{k}_3 + \mathbf{k}_2 - \mathbf{k}_1$ ) in this case:  $\boldsymbol{\kappa}_4 = \mathbf{z}$ ,  $\boldsymbol{\kappa}_3 = \mathbf{x}$ ,  $\boldsymbol{\kappa}_2 = -\mathbf{x}$  and  $\boldsymbol{\kappa}_1 = -\mathbf{z}$ . The signal then depends solely on  $\mathbf{k}_3$  and  $\mathbf{k}_2$ , since  $\mathbf{k}_4$  and  $\mathbf{k}_1$  have only  $z$  components which makes equation (A.11) vanish. Thus, the complete configuration is then  $xyzx(zx\bar{x}\bar{z})$  with  $\bar{\alpha}$  standing for  $-\alpha$ .

**Table 1.** Linearly independent third-order experiments;  $\bar{\alpha} \equiv -\alpha$ .

NC configuration	$F_{\{v\}}^{(4)}$	Dependent wavevectors	Experiment type
<i>xyyy</i>	$(1, 0, 0)^T$	Non	Any
<i>xyxy</i>	$(0, 1, 0)^T$	Non	Any
<i>xyyx</i>	$(0, 0, 1)^T$	Non	Any
CI configuration	$F_{\{v\}}^{(5)}$	Dependent wavevectors	Type
<i>xxxxy</i> (zzzz)	$(0, 0, 0, 0, 1)^T$	$\mathbf{k}_4, \mathbf{k}_3, \mathbf{k}_2, \mathbf{k}_1$	Collinear
<i>xxyx</i> (zzzz)	$(0, 0, 0, 0, 1, 0)^T$	$\mathbf{k}_4, \mathbf{k}_3, \mathbf{k}_2, \mathbf{k}_1$	Collinear
<i>xyxx</i> (zzzz)	$(0, 0, 1, 0, 0, 0)^T$	$\mathbf{k}_4, \mathbf{k}_3, \mathbf{k}_2, \mathbf{k}_1$	Collinear
<i>xxxy</i> (zy $\bar{y}\bar{z}$ )	$(0, 0, 0, 0, 0, 1)^T$	$\mathbf{k}_4, \mathbf{k}_1$	Non-collinear
<i>xxyx</i> (zyzy)	$(0, 0, 0, 0, 1, 0)^T$	$\mathbf{k}_4, \mathbf{k}_2$	Non-collinear
<i>xyxx</i> (zzyy)	$(0, 0, 1, 0, 0, 0)^T$	$\mathbf{k}_4, \mathbf{k}_3$	Non-collinear
<i>xxyz</i> (zzxx)	$(0, 0, 0, 1, 0, 0)^T$	$\mathbf{k}_2, \mathbf{k}_1$	Non-collinear
<i>xyzx</i> (zx $\bar{x}\bar{z}$ )	$(1, 0, 0, 0, 0, 0)^T$	$\mathbf{k}_3, \mathbf{k}_2$	Non-collinear
<i>xyxz</i> (zxzx)	$(0, 1, 0, 0, 0, 0)^T$	$\mathbf{k}_3, \mathbf{k}_1$	Non-collinear

The configuration *xyxz*(zxzx) has *z* polarization of field 1 with  $+\mathbf{k}_1$  directed along *x*, *x* polarization of field 2 with  $+\mathbf{k}_2$  directed along *z*, *y* polarization of field 3 with  $+\mathbf{k}_3$  directed along *x*. This gives a signal  $\mathbf{k}_4$  polarized along *x* and propagating along *z*. Field configurations responsible for other independent contributions [(0, 1, 0, 0, 0, 0)<sup>T</sup>, (0, 0, 1, 0, 0, 0)<sup>T</sup> . . .] can be obtained in the same way. The independent CI techniques are listed in table 1. *xxxxy*(zzzz) and *xxxy*(zy $\bar{y}\bar{z}$ ) differ by the wavevector configuration.

Fourth-rank orientational averaging involving magnetic transition dipoles generates three linearly independent CI field configurations. Six independent configurations are then possible when electric quadrupoles and excitonic contributions are neglected: *xxxxy*(zzzz), *xxyx*(zzzz), *xyxx*(zzzz), *xxxy*(zy $\bar{y}\bar{z}$ ), *xxyx*(zyzy) and *xyxx*(zzyy).

#### 4. Application to photon echo signals in alpha helical polypeptides

We have used the present theory to simulate the 2D signals of alpha helical polypeptides in the amide region covering  $n - \pi^*$  and  $\pi - \pi^*$  electronic transitions. The structure of the 17-residue alpha helix was created using the Macromodel package, and MD simulations were used to generate 100 snapshots along a 10 ns NVE simulation. Detailed description of the structure is given in [63].

We included the backbone amide transitions. Three optical transitions per each amide were considered:  $\pi - \pi^*$  (NV1 and NV2) and  $n - \pi^*$ . Electric dipoles for NV1 and NV2 and magnetic dipoles for  $n - \pi^*$  transition were included as in [6]. To ensure Pauli exclusion we used  $U_{ma,mb} = 10^6 \text{ cm}^{-1}$  ( $U_{ma,nb} = 0$  for  $m \neq n$ ). Electric quadrupoles of the chromophores,  $Q$ , are neglected. Couplings between different amides and amide transition dipoles were obtained using Woody's semiempirical parameters [6].

To estimate the sensitivity of chiral 2D techniques to structural variations we used one snapshot of a typical helical structure (hel). We also created two perturbed structures (figure 1). The first was obtained by restraining the  $\phi$  torsional angle of the ninth residue, which is in the middle of the peptide, to be  $120^\circ$  (the typical value for this angle in an 'ideal' helix is  $53^\circ$ ). A 10 ns NVE ensemble equilibration followed by a 5 ns dynamics run was then carried out to generate one snapshot of the 'twisted' (tw8) helix structure: For the second perturbed

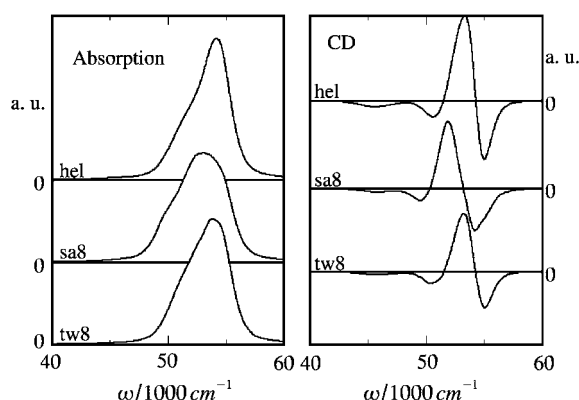


**Figure 2.** Simulated spectra of the 17 residue helices shown in figure 1: absorption (left) and CD (right).

structure an NPT ensemble simulated-annealing was carried out by first gradually raising the temperature from 273 K to 550 K during 5 ns, keeping the temperature for 5 ns and finally cooling down the system from 550 K to 273 K in 5 ns. A 5 ns dynamics run was then performed to generate a single snapshot of the annealed peptide structure (sa8).

The same homogeneous linewidth  $\gamma = 500 \text{ cm}^{-1}$  was assumed for all single-exciton transitions. Inhomogeneous broadening was simulated by ensemble averaging over 100 configurations using a Gaussian distribution of the local peptide excitation energies with variance  $1060 \text{ cm}^{-1}$ , which reproduces the 10 nm Gaussian CD linewidth at 180–240 nm ( $55\,000\text{--}42\,000 \text{ cm}^{-1}$ , respectively).

The absorption spectrum shown in figure 2 has one peak at  $53\,500 \text{ cm}^{-1}$  corresponding to the NV1 transition. The  $n - \pi^*$  transition has no electric transition dipole. However, due to couplings between chromophores it borrows some electric transition dipole from the  $\pi - \pi^*$  transitions; it is very weak and not visible in the absorption due to broad NV1. The CD spectrum has the typical shape for an  $\alpha$  helix: the chiral structure of amides results in strong NV1 transition at  $50\,000\text{--}55\,000 \text{ cm}^{-1}$ , which does not carry a magnetic transition dipole, while the negative peak at  $45\,500 \text{ cm}^{-1}$  is mainly  $n - \pi^*$  transition. The absorption signals of hel, sa8 and tw8 are similar. The negative CD peak at  $45\,000 \text{ cm}^{-1}$  is stronger in hel compared to sa8 and tw8. The CD of all three structures are very similar.

The response function (equation (17)) is a product of two complex Lorentzian functions in  $\Omega_1$  and  $\Omega_3$ . In the dipole approximation the imaginary parts of the response function show localized absorptive-like peaks where peak position correspond to resonances; the real parts of the corresponding contributions are dispersive. This is reversed in the first-order terms in wavevector. Below we display the absorptive lineshapes: imaginary parts of  $xxxx(zzzz)$  and real parts of  $xxxy(zzzz)$ ,  $xxxy(zy\bar{y}\bar{z})$  and  $xyyz(zzxx)$  of the 2D photon echo signal (equation (17)). The signal of hel is displayed in figure 3 for three polarization configurations.  $xxxx(zzzz)$  is NC and shows one pair of strong peaks around  $-\Omega_1 = \Omega_3 = 53\,000 \text{ cm}^{-1}$ . As expected from the absorption, the  $n - \pi^*$  transition at  $-\Omega_1 = \Omega_3 = 45\,000 \text{ cm}^{-1}$  is not visible, but we see a weak off diagonal crosspeaks between these transitions. The CI collinear tensor components,  $xxxy(zzzz)$ ,  $xxxy(zy\bar{y}\bar{z})$  and  $xyyz(zzxx)$ , show extensive redistribution of peak amplitudes: the cross peaks are much stronger than in the NC  $xxxx(zzzz)$ . The differences between various structures are highlighted in the crosspeak regions.

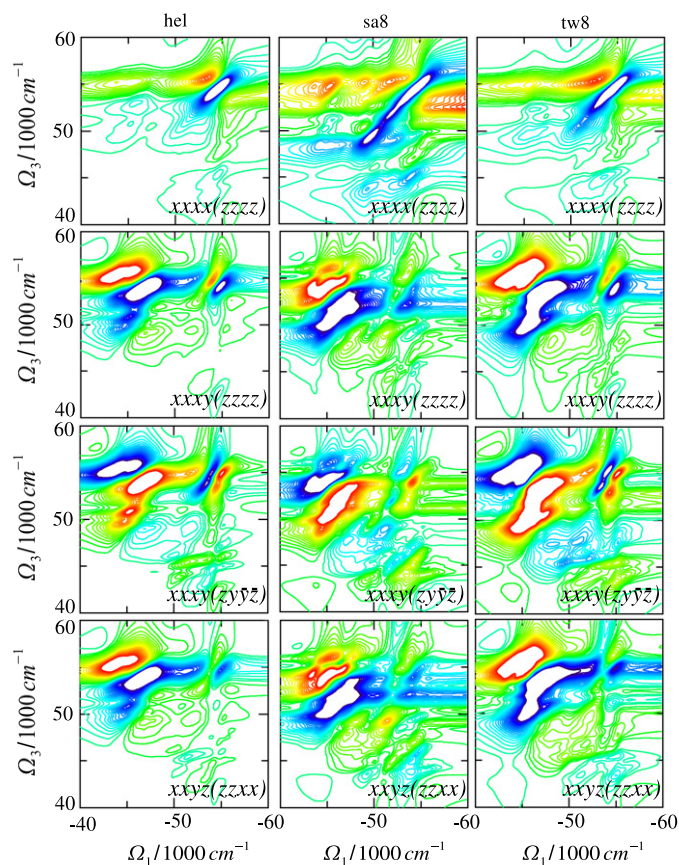


**Figure 3.** Simulated 2D photon echo signals,  $\Re_{v_4 v_3 v_2 v_1}^k(\Omega_3, T_2 = 0, \Omega_1)$ , (equation (17)), shown are the absorptive signals (imaginary part for  $xxxx(zzzz)$  and real part for  $xxxx(zzzz)$ ,  $xxyy(zyyz)$  and  $xxyy(zzxx)$ ) for different optical polarization configurations and polypeptide structures.

## 5. Discussion

The 2D photon echo signals depend on the electric and magnetic transition dipole vectors, the electric quadrupoles, the transition energies and the spatial configuration of chromophores.

Extracting the molecular structure (bond lengths, dihedral angles, etc) is an important goal of multidimensional spectroscopy. The 2D spectrum contains numerous overlapping contributions. The spectrum may not be directly inverted to yield the structure since the number of (linearly independent) unknowns is larger than the number of independent measured quantities. Let us consider the peak intensities and their positions as the measured quantities. In our  $xxxx$  simulation of *hel* we found three pairs of peaks: one close to diagonal and two at crosspeak positions. Their positions along the two frequency axes and their relative intensities could provide  $6 \times 2 + 6 \times 5/2 = 42$  measured parameters. The peak linewidths and their elongation directions provide additional  $6 \times 2 = 12$  parameters. It should thus be possible to extract 54 system parameters out of the data acquired. For comparison, three (two negative and one positive) peaks are typically observed in CD, which is a one-dimensional technique,

of alpha helix. Thus, CD provides  $3 + 3 \times 2/2 + 3 = 9$  parameters. Third-order CI signals provide more structure-sensitive information compared to CD and nonlinear NC techniques.

The peptide with 243 atoms considered here has  $243^3$  coordinates. Our exciton model has 17 chromophores, whose orientations and coordinates are unknown (thus  $17^3 + 17 \times 3 \gg 50$ ). Thus, only a limited number of structural characteristics, e.g. the helicity, the helix length and width, average angles of transition dipoles with the longitudinal helix axis, can be obtained from the spectra.

The expansion of transition currents in electric and magnetic transition multipoles in equation (13) allows us to trace the major contributions to spectroscopic signals. The first two terms are the leading contributions for excitonic systems. The second term is three to four orders of magnitudes smaller than the first and is the main source of the excitonic CD spectrum when the excitons are delocalized among many chromophores. The third and the fourth terms become important in CD spectra of localized excitons. CD of small molecules is usually dominated by the magnetic transition moments expressed through the rotational strength.

The number of linearly independent CI tensor components depends on the specific experimental techniques. For the two pulse photon echo where the second time delay  $t_2 = 0$  the second and third interactions can be interchanged. We then have  $xyyx(zzzz) \equiv xyxx(zzzz)$ ,  $xyyx(zzyy) \equiv xyxx(zzyy)$ ,  $xyyz(zzxx) \equiv xyxz(zxzx)$  leaving six linearly independent tensor components. All nine tensor components should become independent for  $t_2 > 0$ . Specific systems may have fewer components: for example, all tensor components for a two-level chromophore are the same.

Our previous studies were limited to the collinear pulse configurations [45–47]. In this paper we present all independent CI polarization configurations for the third-order nonlinear response. The non-collinear configurations depend on two wavevectors. The NC and CI techniques are identified by their distinct polarization configurations. The simulations presented in figure 3 demonstrate how CI signals may suppress the diagonal peaks, enhancing the resolution of crosspeaks. Chiral techniques are thus very sensitive to the structure and to fine details of the geometry.

## Acknowledgments

This research was supported by the National Science Foundation Grant no CHE-0446555 and the National Institutes of Health 2R01-GM59230-05.

## Appendix. Orientational averagings of molecular properties

Orientational averaging of molecular response tensors is required for randomly oriented bulk systems (e.g. solutions, liquids, polymers, glasses). The tensors associated with one molecule should be averaged over an arbitrary orientation of the molecule with respect to the optical external field. Averaging of the optical response tensors reduces to averaging of products of vectors and tensors as in equation (18). The vector-related averaging is  $\langle \mathbf{d}_N^{\nu_N} \dots \mathbf{d}_j^{\nu_j} \dots \mathbf{d}_1^{\nu_1} \rangle = \text{Average}[(\mathbf{d}_N \cdot \boldsymbol{\nu}_N) \dots (\mathbf{d}_j \cdot \boldsymbol{\nu}_j) \dots (\mathbf{d}_1 \cdot \boldsymbol{\nu}_1)]$ , where vectors  $\mathbf{d}_j$  are the molecular properties given in the molecular frame; the field-related unit vectors  $\boldsymbol{\nu}_j = \mathbf{x}, \mathbf{y}, \mathbf{z}$  are defined in the lab frame. This formula should be slightly modified when one molecular second-rank tensor,  $\mathbf{t}_j^{\nu_j \nu'_j}$ , defined in the molecular frame, is involved:  $\langle \mathbf{d}_N^{\nu_N} \dots \mathbf{t}_j^{\nu_j \nu'_j} \dots \mathbf{d}_1^{\nu_1} \rangle = \text{Average}[(\mathbf{d}_N \cdot \boldsymbol{\nu}_N) \dots (\boldsymbol{\nu}_j \cdot \mathbf{t}_j \cdot \boldsymbol{\nu}'_j) \dots (\mathbf{d}_1 \cdot \boldsymbol{\nu}_1)]$ . This is equivalent to the averaging of  $N + 1$  vectors.

Oriental averaging can be accomplished by introducing the Euler transformation formula for three-dimensional coordinate-system rotations; this leads to integrals of products of trigonometric functions. Alternatively, these averages can be calculated using the matrix formalism developed by Andrews and Thirunamachandran [62], which for two-, three-, four- and five-vector averages gives the following compact expressions:

$$\langle \mathbf{d}_2^{v_2} \mathbf{d}_1^{v_1} \rangle = \frac{1}{3} (\boldsymbol{\nu}_2 \cdot \boldsymbol{\nu}_1) (\mathbf{d}_2 \cdot \mathbf{d}_1) \quad (\text{A.1})$$

$$\langle \mathbf{d}_3^{v_3} \mathbf{d}_2^{v_2} \mathbf{d}_1^{v_1} \rangle = \frac{1}{6} (\boldsymbol{\nu}_3 \cdot (\boldsymbol{\nu}_2 \times \boldsymbol{\nu}_1)) (\mathbf{d}_3 \cdot (\mathbf{d}_2 \times \mathbf{d}_1)) \quad (\text{A.2})$$

$$\langle \mathbf{t}_2^{v'_2} \mathbf{d}_1^{v_1} \rangle = \frac{1}{6} (\boldsymbol{\nu}' \cdot (\boldsymbol{\nu}_2 \times \boldsymbol{\nu}_1)) \mathbf{d}_1 \odot \mathbf{t}_2 \quad (\text{A.3})$$

$$\langle \mathbf{d}_2^{v_2} \mathbf{t}_1^{v'_1} \rangle = \frac{1}{6} (\boldsymbol{\nu}_2 \cdot (\boldsymbol{\nu}' \times \boldsymbol{\nu}_1)) \mathbf{d}_2 \odot \mathbf{t}_1 \quad (\text{A.4})$$

$$\langle \mathbf{d}_4^{v_4} \mathbf{d}_3^{v_3} \mathbf{d}_2^{v_2} \mathbf{d}_1^{v_1} \rangle = F_{\{\nu\}}^{(4)T} M^{(4)} V^{(4)} \quad (\text{A.5})$$

$$\langle \mathbf{t}_4^{v'_4} \mathbf{d}_3^{v_3} \mathbf{d}_2^{v_2} \mathbf{d}_1^{v_1} \rangle = F_{\{\nu\}}^{(5)T} M^{(5)} V_4^{(5)} \quad (\text{A.6})$$

$$\langle \mathbf{d}_4^{v_4} \mathbf{t}_3^{v'_3} \mathbf{d}_2^{v_2} \mathbf{d}_1^{v_1} \rangle = F_{\{\nu\}}^{(5)T} M^{(5)} V_3^{(5)} \quad (\text{A.7})$$

$$\langle \mathbf{d}_4^{v_4} \mathbf{d}_3^{v_3} \mathbf{t}_2^{v'_2} \mathbf{d}_1^{v_1} \rangle = F_{\{\nu\}}^{(5)T} M^{(5)} V_2^{(5)} \quad (\text{A.8})$$

$$\langle \mathbf{d}_4^{v_4} \mathbf{d}_3^{v_3} \mathbf{d}_2^{v_2} \mathbf{t}_1^{v'_1} \rangle = F_{\{\nu\}}^{(5)T} M^{(5)} V_1^{(5)}. \quad (\text{A.9})$$

$F_{\{\nu\}}^{(N)}$  are the column vectors depending on the lab frame unit vectors  $\nu$ :

$$F_{\{\nu\}}^{(4)} = \frac{1}{30} \begin{pmatrix} (\boldsymbol{\nu}_4 \cdot \boldsymbol{\nu}_3)(\boldsymbol{\nu}_2 \cdot \boldsymbol{\nu}_1) \\ (\boldsymbol{\nu}_4 \cdot \boldsymbol{\nu}_2)(\boldsymbol{\nu}_3 \cdot \boldsymbol{\nu}_1) \\ (\boldsymbol{\nu}_4 \cdot \boldsymbol{\nu}_1)(\boldsymbol{\nu}_3 \cdot \boldsymbol{\nu}_2) \end{pmatrix}, \quad (\text{A.10})$$

$$F_{\{\nu\}}^{(5)} = \frac{1}{30} \begin{pmatrix} \boldsymbol{\nu}_4 \cdot (\boldsymbol{\nu}_3 \times \boldsymbol{\nu}_2)(\boldsymbol{\nu}_1 \cdot \boldsymbol{\nu}') \\ \boldsymbol{\nu}_4 \cdot (\boldsymbol{\nu}_3 \times \boldsymbol{\nu}_1)(\boldsymbol{\nu}_2 \cdot \boldsymbol{\nu}') \\ \boldsymbol{\nu}_4 \cdot (\boldsymbol{\nu}_3 \times \boldsymbol{\nu}')(\boldsymbol{\nu}_2 \cdot \boldsymbol{\nu}_1) \\ \boldsymbol{\nu}_4 \cdot (\boldsymbol{\nu}_2 \times \boldsymbol{\nu}_1)(\boldsymbol{\nu}_3 \cdot \boldsymbol{\nu}') \\ \boldsymbol{\nu}_4 \cdot (\boldsymbol{\nu}_2 \times \boldsymbol{\nu}')(\boldsymbol{\nu}_3 \cdot \boldsymbol{\nu}_1) \\ \boldsymbol{\nu}_4 \cdot (\boldsymbol{\nu}_1 \times \boldsymbol{\nu}')(\boldsymbol{\nu}_3 \cdot \boldsymbol{\nu}_2) \end{pmatrix}. \quad (\text{A.11})$$

Matrices  $M$  are system independent:

$$M^{(4)} = \frac{1}{30} \begin{pmatrix} 4 & -1 & -1 \\ -1 & 4 & -1 \\ -1 & -1 & 4 \end{pmatrix}, \quad (\text{A.12})$$

$$M^{(5)} = \frac{1}{30} \begin{pmatrix} 3 & -1 & -1 & 1 & 1 & 0 \\ -1 & 3 & -1 & -1 & 0 & 1 \\ -1 & -1 & 3 & 0 & -1 & -1 \\ 1 & -1 & 0 & 3 & -1 & 1 \\ 1 & 0 & -1 & -1 & 3 & -1 \\ 0 & 1 & -1 & 1 & -1 & 3 \end{pmatrix}, \quad (\text{A.13})$$

and  $V$  are column vectors depending on the system properties:

$$V^{(4)} = \begin{pmatrix} (\mathbf{d}_4 \cdot \mathbf{d}_3)(\mathbf{d}_2 \cdot \mathbf{d}_1) \\ (\mathbf{d}_4 \cdot \mathbf{d}_2)(\mathbf{d}_3 \cdot \mathbf{d}_1) \\ (\mathbf{d}_4 \cdot \mathbf{d}_1)(\mathbf{d}_3 \cdot \mathbf{d}_2) \end{pmatrix}, \quad (\text{A.14})$$

$$V_4^{(5)} = \begin{pmatrix} \mathbf{d}_1 \cdot \mathbf{t}_4 \cdot (\mathbf{d}_3 \times \mathbf{d}_2) \\ \mathbf{d}_2 \cdot \mathbf{t}_4 \cdot (\mathbf{d}_3 \times \mathbf{d}_1) \\ (\mathbf{d}_3 \odot \mathbf{t}_4)(\mathbf{d}_2 \cdot \mathbf{d}_1) \\ \mathbf{d}_3 \cdot \mathbf{t}_4 \cdot (\mathbf{d}_2 \times \mathbf{d}_1) \\ (\mathbf{d}_2 \odot \mathbf{t}_4)(\mathbf{d}_3 \cdot \mathbf{d}_1) \\ (\mathbf{d}_1 \odot \mathbf{t}_4)(\mathbf{d}_3 \cdot \mathbf{d}_2) \end{pmatrix}, \quad (\text{A.15})$$

$$V_3^{(5)} = \begin{pmatrix} \mathbf{d}_1 \cdot \mathbf{t}_3 \cdot (\mathbf{d}_2 \times \mathbf{d}_4) \\ \mathbf{d}_2 \cdot \mathbf{t}_3 \cdot (\mathbf{d}_1 \times \mathbf{d}_4) \\ -(\mathbf{d}_4 \odot \mathbf{t}_3)(\mathbf{d}_2 \cdot \mathbf{d}_1) \\ \bar{\mathbf{t}}_3(\mathbf{d}_4 \cdot (\mathbf{d}_2 \times \mathbf{d}_1)) \\ (\mathbf{d}_4 \times \mathbf{d}_2) \cdot \mathbf{t}_3 \cdot \mathbf{d}_1 \\ (\mathbf{d}_4 \times \mathbf{d}_1) \cdot \mathbf{t}_3 \cdot \mathbf{d}_2 \end{pmatrix}, \quad (\text{A.16})$$

$$V_2^{(5)} = \begin{pmatrix} \mathbf{d}_1 \cdot \mathbf{t}_2 \cdot (\mathbf{d}_4 \times \mathbf{d}_3) \\ \bar{\mathbf{t}}_2(\mathbf{d}_4 \cdot (\mathbf{d}_3 \times \mathbf{d}_1)) \\ (\mathbf{d}_4 \times \mathbf{d}_3) \cdot \mathbf{t}_2 \cdot \mathbf{d}_1 \\ \mathbf{d}_3 \cdot \mathbf{t}_2 \cdot (\mathbf{d}_1 \times \mathbf{d}_4) \\ -(\mathbf{d}_4 \odot \mathbf{t}_2)(\mathbf{d}_3 \cdot \mathbf{d}_1) \\ (\mathbf{d}_4 \times \mathbf{d}_1) \cdot \mathbf{t}_2 \cdot \mathbf{d}_3 \end{pmatrix}, \quad (\text{A.17})$$

$$V_1^{(5)} = \begin{pmatrix} \bar{\mathbf{t}}_1(\mathbf{d}_4 \cdot (\mathbf{d}_3 \times \mathbf{d}_2)) \\ \mathbf{d}_2 \cdot \mathbf{t}_1 \cdot (\mathbf{d}_4 \times \mathbf{d}_3) \\ (\mathbf{d}_4 \times \mathbf{d}_3) \cdot \mathbf{t}_1 \cdot \mathbf{d}_2 \\ \mathbf{d}_3 \cdot \mathbf{t}_1 \cdot (\mathbf{d}_4 \times \mathbf{d}_2) \\ (\mathbf{d}_4 \times \mathbf{d}_2) \cdot \mathbf{t}_1 \cdot \mathbf{d}_3 \\ -(\mathbf{d}_4 \odot \mathbf{t}_1)(\mathbf{d}_3 \cdot \mathbf{d}_2) \end{pmatrix}. \quad (\text{A.18})$$

where  $\mathbf{d} \odot \mathbf{t} \equiv \sum_{\alpha_3 \alpha_2 \alpha_1} \epsilon_{\alpha_3 \alpha_2 \alpha_1} \mathbf{d}^{\alpha_3} \mathbf{t}^{\alpha_2 \alpha_1}$ ,  $(\mathbf{t} \cdot \mathbf{d})^\alpha \equiv \sum_{\alpha'} \mathbf{t}^{\alpha \alpha'} \mathbf{d}^{\alpha'}$ ,  $(\mathbf{d} \cdot \mathbf{t})^\alpha \equiv \sum_{\alpha'} \mathbf{d}^{\alpha'} \mathbf{t}^{\alpha' \alpha}$  and  $\bar{\mathbf{t}} \equiv \sum_{\alpha} \mathbf{t}^{\alpha \alpha}$ , consequently  $\mathbf{d}_1 \cdot \mathbf{t} \cdot \mathbf{d}_2 \equiv \sum_{\alpha_1 \alpha_2} \mathbf{d}_1^{\alpha_1} \mathbf{t}^{\alpha_1 \alpha_2} \mathbf{d}_2^{\alpha_2}$ .

By comparing with equation (18), we can calculate the orientational averaging of currents by replacing vectors  $\mathbf{d}$  with  $\boldsymbol{\mu}$  and  $\mathbf{m}$  and tensors  $\mathbf{t}$  with quadrupoles  $\mathbf{q}$ .

## References

- [1] Lough W J and Wainer I W (ed) 2002 *Chirality in Natural and Applied Science* (Boca Raton, FL: CRC Press)
- [2] Barron L D 2004 *Molecular Light Scattering and Optical Activity* 2nd edn (Cambridge: Cambridge University Press)
- [3] Buckingham A D and Fischer P 2002 Optical response of a chiral liquid *Chirality (Physical Chemistry)* ed J M Hicks (Oxford: Oxford University Press) pp 119–29
- [4] Berova N, Nakanishi K and Woody R W (ed) 2000 *Circular Dichroism: Principles and Applications* 2nd edn (New York: Wiley)
- [5] Nafie L A 1997 *Annu. Rev. Phys. Chem.* **48** 357
- [6] Woody R W and Sreerama N 1999 *J. Chem. Phys.* **111** 2844

- [7] Chin D H, Woody R W, Rohl C A and Baldwin R L 2002 *Proc. Natl Acad. Sci. USA* **99** 15416
- [8] Sreerama N and Woody R W 2003 *Protein Sci.* **12** 384
- [9] Woody R W 2005 *Monatshefte für Chemie* **136** 347
- [10] Eker F, Cao X, Nafie L A, Huang Q and Schweitzer-Stenner R 2003 *J. Phys. Chem. B* **107** 358
- [11] Hilario J, Kubelka J, Syud F A, Gellman T A and Keiderling S H 2002 *Biopolymers* **67** 233
- [12] Hilario J, Kubelka J and Keiderling T A 2003 *J. Am. Chem. Soc.* **125** 7562
- [13] Barron L D, Blanch E W, McColl I H, Syme C D, Hecht L and Nielsen K 2003 *Spectroscopy* **17** 101
- [14] McColl I H, Blanch E W, Gill A C, Rhie A G O, Ritchie L, Hecht M A, Nielsen K and Barron L D 2003 *J. Am. Chem. Soc.* **125** 10019
- [15] Andrews D L and Allcock P 2002 *Optical Harmonics in Molecular Systems* (New York: Wiley)
- [16] Byers J D, Yee H I and Hicks J M 1994 *J. Chem. Phys.* **101** 6233
- [17] Hicks J M, Petralli-Mallow T and Byers J D 1994 *Faraday Discuss.* **99** 341
- [18] Freund I and Rentzepis P M 1967 *Phys. Rev. Lett.* **18** 393
- [19] Moad A J and Simpson G J 2004 *J. Phys. Chem. B* **108** 3548
- [20] Simpson G J 2002 *J. Chem. Phys.* **117** 3398
- [21] Simpson G J and Rowlen K L 2000 *Acc. Chem. Res.* **33** 781
- [22] Fischer P, Beckwitt K, Wise F W and Albrecht A C 2002 *Chem. Phys. Lett.* **352** 463  
Fischer P, Buckingham A D and Albrecht A C 2001 *Phys. Rev. A* **64** 053816  
Fisher P, Wise F W and Albrecht A C 2003 *J. Phys. Chem. A* **107** 8232
- [23] Koroteev N I, Makarov V A and Volkov S N 1998 *Opt. Commun.* **157** 111
- [24] Lakhtakia A 2006 *Phys. Lett. A* **354** 330
- [25] Cho M and Fleming G R 2005 *J. Chem. Phys.* **123** 114506
- [26] Prall B S, Parkinson D Y and Fleming G R 2005 *J. Chem. Phys.* **123** 054515
- [27] Fang C, Wang J, Kim Y S, Charnley A K, Barber-Armstrong W, Smith A B III, Decatur S M and Hochstrasser R M 2004 *J. Phys. Chem. B* **108** 10415
- [28] Rubstov I V, Wang J and Hochstrasser R M 2003 *Proc. Natl Acad. Sci. USA* **100** 5601
- [29] Mukamel S 2000 *Annu. Rev. Phys. Chem.* **51** 691
- [30] Larsen D S, Vengris M, van Stokkum I H M, van der Horst M A, de Weerd F L, Hellingwerf K J and van Grondelle R 2004 *Biophys. J.* **86** 2538
- [31] Larsen O F A, van Stokkum I H M F L, de Weerd V M, Aravindakumar C T, van Grondelle R, Geacintov N E and van Amerongen H 2004 *Phys. Chem. Chem. Phys.* **6** 154
- [32] Demidöven N, Cheatum C M, Chung H S, Khalil M, Knoester J and Tokmakoff A 2004 *J. Am. Chem. Soc.* **126** 7981
- [33] Cowan M L, Bruner B D, Huse N, Dwyer J R, Chugh B, Nibbering E T J, Elsaesser T and Miller R J D 2005 *Nature* **434** 199
- [34] Fecko C J, Eaves J D, Loparo J J, Tokmakoff A and Geissler P L 2003 *Science* **301** 1698
- [35] Chi Z, Chen X G, Holtz S W and Asher S A 1998 *Biochemistry* **37** 2854
- [36] Mikhonin A V, Myshakina N S, Bykov S V and Asher S A 2005 *J. Am. Chem. Soc.* **127** 7712
- [37] Pimenov K V, Bykov S V, Mikhonin A V and Asher S A 2005 *J. Am. Chem. Soc.* **127** 2840
- [38] Moran A M, Park S-M, Dreyer J and Mukamel S 2003 *J. Chem. Phys.* **118** 3651
- [39] Piryatinski A, Chernyak V and Mukamel S 2001 *Chem. Phys.* **266** 311
- [40] Zanni M T, Ge N-H, Kim Y S and Hochstrasser R M 2001 *Proc. Natl Acad. Sci. USA* **98** 11265
- [41] Fulmer E C, Mukherjee P, Krummel A T and Zanni M T 2004 *J. Chem. Phys.* **120** 8067
- [42] Demirdoven N, Khalil M and Tokmakoff A 2002 *Phys. Rev. Lett.* **89** 237401
- [43] Venkatramani R and Mukamel S 2002 *J. Chem. Phys.* **117** 11089
- [44] Zhuang W, Abramavicius D and Mukamel S 2005 *Proc. Natl Acad. Sci. USA* **102** 7443
- [45] Abramavicius D and Mukamel S 2005 *J. Chem. Phys.* **122** 134305
- [46] Abramavicius D and Mukamel S 2006 *J. Chem. Phys.* **124** 034113
- [47] Abramavicius D and Mukamel S 2005 *Chem. Phys.* **318** 50
- [48] Craig D P, Power E A and Thirunamachandran T 1974 *Chem. Phys. Lett.* **27** 149
- [49] Cohen-Tannoudji C, Dupont-Roc J and Grynberg G 1992 *Atom-Photon Interactions* (New York: Wiley)
- [50] Mukamel S 1995 *Principles of Nonlinear Optical Spectroscopy* (New York: Oxford University Press)
- [51] Craig D P and Thirunamachandran T 1998 *Molecular Quantum Electrodynamics. An Introduction to Radiation Molecule Interactions* (New York: Dover)
- [52] Woolley R G 1974 *J. Phys. B: At. Mol. Phys.* **7** 488
- [53] Tanaka S, Chernyak V and Mukamel S 2001 *Phys. Rev. A* **63** 063405
- [54] Woody R W 1968 *J. Chem. Phys.* **49** 4797
- [55] Hirst J D 1998 *J. Chem. Phys.* **109** 782

- 
- [56] Sreerama N, Venyaminov S Y and Woody R W 2000 *Anal. Biochem.* **287** 243
- [57] Davydov A 1962 *A Theory of Molecular Excitations* (New York: McGraw-Hill)
- [58] van Amerongen H, Valkunas L and van Grondelle R 2000 *Photosynthetic Excitons* (Singapore: World Scientific)
- [59] Mukamel S and Abramavicius D 2004 *Chem. Rev.* **104** 2073
- [60] Leegwater J A and Mukamel S 1992 *Phys. Rev. A* **46** 452
- [61] Chernyak V, Zhang W M and Mukamel S 1998 *J. Chem. Phys.* **109** 9587
- [62] Andrews D L and Thirunamachandran T 1977 *J. Chem. Phys.* **67** 5026
- [63] Zhuang W, Abramavicius D, Hayashi T and Mukamel S 2006 *J. Phys. Chem. B* **110** 3362